Cancer Nano (2012) 3:65–81
DOI 10.1007/s12645-012-0031-2

ORIGINAL PAPER

Apoptosis-induced anticancer effect of transferrin-conjugated solid lipid nanoparticles of curcumin

Rohit S. Mulik · Jukka Mönkkönen · Risto O. Juvonen · Kakasaheb R. Mahadik · Anant R. Paradkar

Received: 24 September 2012 / Accepted: 16 October 2012 / Published online: 13 November 2012

Abstract Broad spectrum therapeutic potential of curcumin is usually hampered by its photodegradation and low bioavailability. Present investigation was designed with an objective to develop transferrin-mediated solid lipid nanoparticles (Tf-C-SLN) resistant to the photostability and capable of enhancing the bioavailability by targeted drug delivery to elicit anticancer activity against SH-SY5Y neuroblastoma cells in vitro. Hot homogenization method was used for the formulation of Tf-C-SLN and evaluated physicochemically using parameters such as, size, zeta potential, entrapment efficiency and photostability, transmission electron microscopy (TEM), nuclear magnetic resonance (NMR), differential scanning colorimetry (DSC), and in vitro release study. In vitro cytotoxicity and apoptosis investigations were performed using microplate analysis and flow cytometry techniques. The physicochemical characterization confirmed the suitability of formulation method and various parameters therein. TEM investigation revealed the spherical morphology while NMR and DSC study confirmed the entrapment of curcumin inside the nanoparticles. The cytotoxicity, reactive oxygen species, and cell uptake were found to be increased considerably with Tf-C-SLN compared with curcumin-solubilized surfactant solution, and curcumin-loaded SLN (C-SLN) suggesting the targeting effect. AnnexinV-FITC/PI double staining, DNA analysis, caspase detection, and reduced mitochondrial potential confirmed the induction of apoptosis with nanoparticle treatment. Enhanced anticancer activity with Tf-C-SLN compared with curcumin-solubilized surfactant solution and C-SLN was observed from flow cytometry investigations with apoptosis being the major underlying mechanism. The in vitro observations of our investigation are very compelling and concrete to advocate the potential of Tf-C-SLN in enhancing the anticancer effect of curcumin against neuroblastoma in vivo and possible clinical applications.

Electronic supplementary material The online version of this article (doi:10.1007/s12645-012-0031-2) contains supplementary material, which is available to authorized users.

R. S. Mulik · K. R. Mahadik
Department of Pharmaceutics, Poona College of Pharmacy,
Bharati Vidyapeeth University,
Erandwane,
Pune 411038, India

R. S. Mulik
e-mail: rohitmulik@gmail.com

A. R. Paradkar (✉)
Centre for Pharmaceutical Engineering Science,
University of Bradford,
Bradford BD7 1DP, UK
e-mail: A.Paradkar1@bradford.ac.uk

R. S. Mulik · J. Mönkkönen
Department of Biopharmacy, School of Pharmacy,
University of Eastern Finland,
P.O. Box 1627, 70211 Kuopio, Finland

R. S. Mulik · R. O. Juvonen
Department of Toxicology, School of Pharmacy,
University of Eastern Finland,
P.O. Box 1627, 70211 Kuopio, Finland

Present Address:
R. S. Mulik
Advanced Imaging Research Center, University of Texas
Southwestern Medical Center,
5323 Harry Hines Boulevard,
Dallas, TX 75390, USA

Keywords Curcumin · Solid lipid nanoparticles · Neuroblastoma · Flow cytometry · Apoptosis

1 Introduction

There has been tremendous interest for the use of phytoconstituents in the scientific community to combat two of the most lethal diseases in the world today, cardiovascular disease and cancer (Sharma et al. 2005). One such dietary component derived from dried ground rhizome of the perennial herb *Curcuma longa* Linn is turmeric. Turmeric contains turmerin, essential oils, and curcuminoids including curcumin (Sharma et al. 2005). Curcumin has been the subject of hundreds of published papers over the past three decades owing to its wide range of therapeutic efficacy such as, antioxidant, anti-inflammatory, antimicrobial, wound healing, cancer chemopreventive, and potentially chemotherapeutic properties (Aggarwal et al. 2005a; Aggarwal and Harikumar 2009; Anand et al. 2008; Chattopadhyay et al. 2004). Numerous investigations have already confirmed the strong therapeutic potential of curcumin against cancers of various origins such as, skin, prostate, ovarian, colon, breast, brain, blood, liver, and pancreas being completely harmless to normal healthy cells at the same time in total contrast to chemotherapy (Aggarwal et al. 2003a; Azuine and Bhide 1992; Ramachandran et al. 2002; Dorai et al. 2001). The mechanism of anticancer activity of curcumin is not yet fully elucidated. However, few mechanisms have been proposed in the past investigations such as, cell cycle inhibition, signal transduction modulation resulting in gene expression alterations, and apoptosis (Aggarwal et al. 2003b; Joe et al. 2004; Thangapazham et al. 2006). It has been demonstrated recently that cell cycle inhibition and induction of apoptosis are the main underlying mechanisms involved in anticancer activity of curcumin (Aggarwal et al. 2003a, b; Joe et al. 2004; Thangapazham et al. 2006). Generation of reactive oxygen species (ROS) (Buttke and Sandstrom 1994; Jacobson 1996; Christine et al. 2004) and inhibition of NFkB being the main pathways involved in the induction of apoptosis (Aggarwal et al. 2005b; Singh and Aggarwal 1995). Moreover, it has been scientifically proved that curcumin imparts its anticancer effect by acting against all three stages of carcinogenesis (i.e., initiation, progression, and promotion) affecting specific signaling cascade target (Aggarwal et al. 2003a, b). Despite of tremendous therapeutic potential of curcumin against cancer including neuroblastoma, low bioavailability, short half life, and photodegradation are the major limiting factors of curcumin its overall therapeutic efficacy (Aggarwal et al. 2003a, b; Anand et al. 2007; Ansari et al. 2005). We have developed transferrin (Tf)-mediated solid lipid nanoparticles (Tf-C-SLN) encapsulating curcumin which can effectively increase the bioavailability and half life of curcumin by tumor-specific uptake and protecting it from photodegradation at the same time. Hence, the rationale of present investigation was to overcome these limiting factors to improve the therapeutic efficacy of curcumin.

Overexpression of Tf receptor in malignant tissues compared with normal tissues because of the higher iron demand of malignant cells for fast growth and division is well known resulting in the shift of scientific attention towards Tf-mediated drug and gene delivery systems in the past few years for cancer targeting (Widera et al. 2003; Qian et al. 2002). For example, Tf-conjugated PLGA nanoparticles containing paclitaxel for enhanced antiproliferative activity (Sahoo and Labhasetwar 2005), Tf-PEG liposomes for intracellular delivery and targeting to solid tumors (Maruyama et al. 2004), Tf-conjugated gold nanoparticles for cancer cell imaging and therapy (Li et al. 2009), Tf-conjugated PEG–albumin nanoparticles for brain targeting (Ulbrich et al. 2009), Tf receptor-targeted lipid nanoparticles for delivery of an antisense oligodeoxyribonucleotide against Bcl-2 (Yang et al. 2009), Tf-conjugated curcumin-loaded super paramagnetic iron oxide nanoparticles against leukemia (Dilnawaz et al. 2012), etc. There are few reports based on targeted siRNA, peptide, protein, and plasmid delivery systems for the treatment of neuroblastoma (Adrian et al. 2011; Di Paolo et al. 2011; Veldhoen et al. 2008; Tivnan et al. 2012; Dehal et al. 2002). However, investigations based on targeted drug delivery of curcumin for neuroblastoma and elucidation of possible underlying mechanisms of its anticancer activity against neuroblastoma is unexplored till date.

Most of the lipophilic molecules cannot cross the blood–brain barrier (BBB) by free diffusion barring few exceptions. All these molecules require specialized targeted drug delivery systems to be able to cross the BBB in the treatment of brain disorders including cancer (Gutman et al. 2000). Overexpression of Tf receptor on the surface of SH-SY5Y neuroblastoma cells is well documented (Martell et al. 1993). The main objective of the present study was to formulate stable Tf-conjugated solid lipid nanoparticles containing curcumin for the targeted delivery to neuroblastoma cells and evaluate its enhanced anticancer effect in vitro. The distinct advantages of prepared formulation are biodegradable and biocompatible delivery system, tumor cell specific uptake of curcumin by receptor-mediated endocytosis, sustained release of encapsulated curcumin, increased retention time and, hence, increased therapeutic efficacy. Being *p*-glycoprotein inhibitors, both transferrin (Tf) (Wang et al. 2000; Lemieux and Page 1994) and curcumin (Chearwae et al. 2006; Chearwae et al. 2004) can bypass membrane-associated efflux transporters leading to increased intracellular uptake and retention of the drug.

2 Materials and methods

2.1 Materials

Hydrogenated soya phosphatidylcholine (HSPC), distearoyl phosphatidyl ethanolamine (DSPE), and cholesterol (Chol) were purchased from Lipoid. Triolein was purchased from Sigma Aldrich, USA. Transferrin (Human, low endotoxin) was purchased from Calbiochem, USA. Curcumin was a kind gift from Indsaaf Inc., Batala, India. 1-ethyl-3-[3-dimethylaminopropyl] carbodiimide hydrochloride (EDC) and coomassie brilliant blue G dye were purchased from Himedia, Mumbai, India. AnnexinV-FITC and propidium iodide were purchased from Biolegend Europe BV, Netherlands. 2′,7′-dichlorodihydrofluorescein diacetate (H2DCFDA), tetramethyl rhodamine methyl ester were purchased from Sigma Aldrich, Germany. Growth medium RPMI 1640 was purchased from BioWhittaker Inc. (Lonza, Belgium). 3-(4,5-dimethylthiazol-2-yl)-2,5-diphenyl tetrazolium bromide (MTT) was purchased from Sigma Aldrich, Germany. All aqueous solutions were prepared with distilled and deionized water. All other reagents and chemicals used were of analytical grade.

2.2 Methods

2.2.1 Preparation of curcumin-loaded solid lipid nanoparticles

The SLN were prepared by a method as described previously (Gupta et al. 2007; Mulik et al. 2010). In brief, HSPC/DSPE/Chol/triolein (1.5:1:1.2:1; *w*/*w*) were melted at 80 °C. Curcumin was dissolved in ethanol separately and added to lipid melt phase at 80 °C. Melt phase was injected rapidly to the aqueous phase (0.1 % *w*/*v* poloxamer 188, 80 °C) using Ultraturrax high-speed homogenizer at 25,000 rpm speed and homogenized for 15 min. The obtained hot premix was then passed through high pressure homogenizer at 800 bar pressure for 10 cycles at 80 °C. The suspension was immediately cooled to 4–8 °C after homogenization and filtered through 0.2 μm polyethersulfone membrane filter. The pellets of nanoparticles were formed using ultracentrifugation at 25,000×*g* for 30 min at 4 °C and resuspended in distilled water for lyophilization (LyoPro 3000, Heto-Holten A/S, Allerod, Denmark) using mannitol as a cryoprotectant.

2.2.2 Conjugation of Tf to C-SLN

Covalent coupling of Tf by its carboxyl group to the amino group of DSPE present on the surface of curcumin-loaded solid lipid nanoparticles (C-SLN) was carried out using EDC coupling reaction through amide bond formation as described previously (Gupta et al. 2007; Mulik et al. 2010). Unbound Tf was removed from Tf-C-SLN by centrifugation using Avanti J-301 centrifuge (Beckman Coulter, USA) at 25,000×*g* for 10 min.

2.2.3 Characterization of SLN

Optimization of preparation of SLN The preparation of SLN was optimized using 3^2 factorial design. The variables were determined from the preliminary experiments. The weight ratio of lipids and amount of stabilizer were taken as independent variables and their effect on dependent variables such as, particle size, zeta potential, and percent drug entrapment (PDE) was investigated for optimization (Padamwar and Pokharkar 2006). The particle size of C-SLN and Tf-C-SLN was determined using dynamic light scattering with Malvern Hydro 2000 SM particle size analyzer (Malvern Instruments, UK). For the measurement, the laser obscuration range was maintained between 2 and 5 % (Page-Clisson et al. 1998). Homogeneous size distribution was confirmed from the polydispersity index (PdI). The zeta potential was measured by Laser Doppler Velocimetry using Zetasizer 3000, Malvern Instruments, Malvern, UK at 25 °C. The entrapment efficiency of SLN was determined using the ultracentrifugation method at 18,000×*g* for 30 min (Beckmann TL-100, MN) (Jenning et al. 2000). In brief, the pellets of SLN were obtained by ultracentrifugation at 18,000×*g* for 30 min, supernatant was decanted, and curcumin was extracted from the pellets using ethanol. The lyses solution was further diluted with phosphate-buffered saline (PBS) at pH 7.4 and analyzed for curcumin content using ultraviolet–visible (UV–vis) spectrophotometer (V-530, Jasco, Japan) at 424 nm.

Characterization of optimized C-SLN and Tf-C-SLN Bradford assay using coomassie blue G (Bradford 1976) was used for the quantification of conjugation of Tf on the surface of the C-SLN as per our published research (Mulik et al. 2010). Conjugation efficiency is expressed as milligrams of Tf per millimolar of phospholipids. Transmission electron microscopy (TEM) was performed using Hitachi S-7500 transmission electron microscope (Hitachi, Japan) to determine morphological characteristics and particle size of both the SLN (Mulik et al. 2010).

Stability study The stability of curcumin in curcumin-solubilized surfactant solution (CSSS) and C-SLN was studied for 6 months at 40 °C temperature and 75 % relative humidity in the presence of light by determining the drug content using HPLC method coupled with UV–vis detector as previously described (Mulik et al. 2010).

Change in particle size and zeta potential of SLN was also observed over a period of 6 months to determine physical stability of SLN.

2.3 1H NMR study

Nuclear magnetic resonance (NMR) spectra of CSSS, blank solid lipid nanoparticles (B-SLN), and C-SLN were obtained using Varian (Mercury YH-300 MHz) NMR instrument using CDCl3 (Merck, Germany) as a solvent and tetramethylsilane as an internal standard. The samples dissolved in CDCl3 were spinned at 20 RPS at a power level of −5 db. The pulse length was 5 μs with a delay time of 10 s. NMR chemical shifts (δ) are reported in parts per million (Mulik et al. 2009; Reddy and Murthy 2004).

2.4 Differential scanning colorimetry of nanoparticles

Thermal analysis of CSSS, B-SLN, and C-SLN was used to provide additional information on the lipid–drug relationship and the nature of formed nanoparticles (Jenning et al. 2000 and Tiyaboonchaia et al. 2007). A Mettler Toledo DSC 821e equipped with an intracooler (Mettler Toledo, Switzerland) was used for characterization with a 5 mg sample in hermetically sealed aluminium pans heated from 25 to 300 °C at a constant rate of 10 °C/min. Inert atmosphere was maintained by nitrogen purging at a flow rate of 20 ml/min.

2.5 Cell culture study

SH-SY5Y human neuroblastoma cells were obtained from American Type Culture Collection (ATCC, Manassas, VA). The cells were grown in DMEM medium supplemented with 10 % fetal bovine serum and 1 % penicillin G-streptomycin (Gibco BRL, Grand Island, NY) at 37 °C in a humidified, 5 % CO_2 atmosphere in a CO_2 incubator.

2.6 MTT assay

SH-SY5Y Cells (2×10^4/well) were seeded in a 96-well plate and allowed to attach for 24 h. Then the medium was replaced with fresh medium and the cells were treated with different concentrations of CSSS, C-SLN and Tf-C-SLN (2, 4, 8, 16, 32, and 64 μM curcumin/well) using surfactant solution (SS) and B-SLN as the respective controls and incubated for 24 h at 37 °C in CO_2 incubator. After the treatment, medium was removed, cells were washed three times with PBS and fresh medium was added. Then, 25 μl of MTT (5 mg/ml in PBS) was added to the cells and incubated for 3 h at 37 °C in CO_2 incubator. MTT gets reduced to purple formazan in living cells by mitochondrial reductase. This reduction takes place only when reductase enzymes are active, and therefore this conversion is used as a measure of viable (living) cells. Then, the cells were lysed and the dark blue crystals were solubilized with 125 μl of a lysis solution (50 % (*v*/*v*) *N*,*N*,dimethylformamide and 20 % (*w*/*v*) sodium dodecylsulphate, pH 4.5). The optical density of each well was measured with a Victor 1420 Multilabel Counter (PerkinElmer Life Sci., USA) equipped with a 570-nm filter. Percent of cell survival was defined as the relative absorbance of treated cells vs. respective controls. Results were expressed as percent viability vs. dose.

Receptor blocking experiment was carried out to confirm receptor-mediated endocytosis of Tf-C-SLN. Cell surface receptors were blocked by incubating the cells with an excess amount of free Tf for 1 h prior to incubation with Tf-C-SLN, and the effect on cell viability was determined after 24 h treatment (Sahoo and Labhasetwar 2005). For this experiment, 4 μM dose of curcumin was used.

The effect on cell viability with treatment of different time intervals was also assessed. In brief, the cells (1×10^5/well) were seeded in 24-well plate and allowed to attach for 24 h. Then, the medium was replaced with fresh medium and treated with CSSS, C-SLN and Tf-C-SLN (4 μM curcumin/well) using SS and B-SLN as the respective controls and incubated at 37 °C in CO_2 incubator for 3, 6, 12, 24, and 48 h and the effect on cell viability was determined as described above. Results were expressed as percent cell viability vs. time.

2.7 Cell uptake study

Intracelllar uptake of curcumin by SH-SY5Y cells treated with CSSS, C-SLN, and Tf-C-SLN was evaluated using fluorescence microscopy (Weir et al. 2007) and spectrophotometry (Kunwar et al. 2008). For quantitative cell uptake, the cells were treated as described above (10 μM curcumin/well) for different time intervals (3, 6, 12, 24, and 48 h). At each time point, the cells were trypsinized and centrifuged for 3 min at 3,000 rpm. Cell pellets were resuspended in 1 ml methanol and vortexed for 5 min to extract curcumin in methanol fraction. The lysate was then centrifuged at 5,000 rpm for 5 min and absorbance of supernatant containing methanolic curcumin was measured at 428 nm using UV–vis spectrophotometer (V-530, Jasco, Japan). From the calibration plot of methanolic curcumin at 428 nm, the amount of curcumin loading into the cells was determined (Kunwar et al. 2008). The effect on Tf receptor blocking on cell uptake of Tf-C-SLN was also assessed after 24 h treatment with 10 μM curcumin. The uptake of curcumin was expressed as μg of curcumin per 10^5 cells.

For qualitative estimation of uptake of curcumin by cells, the autofluorescence of curcumin was observed using fluorescence microscopy. Cells (1×10^5/well) were

seeded in 24-well plate and allowed to attach for 24 h. By replacing the medium with fresh medium, cells were treated with CSSS, C-SLN and Tf-C-SLN (20 μM curcumin/well) for different time intervals (6, 12, 24, and 48 h). After each time interval, fresh medium was added by prewashing the cells thrice with PBS and fluorescence images of curcumin were captured using Nikon Eclipse TE300 fluorescence microscope with Nikon F601 camera (Nikon, Japan).

2.8 Measurement of ROS

The formation of ROS was evaluated by means of the probe 2′,7′-dichlorodihydrofluorescein diacetate (H2DCF-DA) as described previously (Wang and Joseph 1999). Briefly, SH-SY5Y cells (2×10^4/well) were seeded into 96-well plates and allowed to attach for 24 h. After 24 h, fresh medium was added and cells were treated for 24 h at 37 °C in CO_2 incubator with different concentrations of CSSS, C-SLN, and Tf-C-SLN (2, 4, 8, 16, 32, and 64 μM curcumin/well) using SS and B-SLN as the respective controls. After treatment, cells were washed thrice with PBS; H2DCF-DA was added (10 μM) and incubated for 2 h at 37 °C. H2DCF-DA passively diffuses into cells to get converted to H2DCF by intracellular esterases and gets entrapped within the cell. H2DCF get rapidly oxidized to the highly fluorescent 2′,7′-dichlorofluorescein in presence of intracellular ROS. Fluorescence intensity was measured at an excitation wavelength of 502 nm and an emission wavelength of 520 nm using Envision 2104 Multilabel Reader (PerkinElmer Life Sci, USA).

In receptor blocking experiment, cell surface Tf receptors were blocked by incubating cells with an excess amount of free Tf for 1 h prior to incubation with Tf-C-SLN and the effect on ROS generation was determined after 24 h treatment (Sahoo and Labhasetwar 2005). For this experiment, 4 μM dose of curcumin was used.

The effect of time of treatment on the generation of ROS was also evaluated. In brief, the cells (1×10^5/well) were seeded in 48-well plate and allowed to attach for 24 h. Fresh medium was added to the cells and treated with CSSS, C-SLN, and Tf-C-SLN (4 μM curcumin/well) using SS and B-SLN as the respective controls for 3, 6, 12, 24, and 48 h at 37 °C in CO_2 incubator. Generation of ROS at different time intervals was determined as described above. Results were expressed as relative fluorescence unit vs. time.

2.9 Cell death analysis

In early apoptotic stage phosphatidylserine (PS) makes way to the outer plasma membrane leaflet. Annexin V-FITC has the ability to bind specifically to PS with high affinity while propidium iodide (PI) conjugates to necrotic cells (Ganta and Amiji 2009). Hence, double staining with annexin V-FITC and PI to detect apoptotic and necrotic cells was performed. SH-SY5Y cells (1×10^6/75 cm^2 flask) were seeded and allowed to attach for 24 h. Fresh medium was added and cells were treated with CSSS, C-SLN, and Tf-C-SLN (2 and 4 μM curcumin/well) using SS and B-SLN as the respective controls for 24 and 48 h at 37 °C in CO_2 incubator. Cells were collected by trypsinization after treatment, suspended in a fresh medium, and washed with PBS two to three times. Finally, cell pellets were resuspended in Annexin V binding buffer (1×10^6/ml), 100 μl of this cell suspension was stained with 5 μl AnnexinV-FITC and 10 μl PI and incubated for 15 min in dark at room temperature. Finally, 400 μl of Annexin V binding buffer was added. Treated unstained cells (1×10^6/ml) were used as a positive control to detect the possible autofluorescence of curcumin in green (FL1) channel. Approximately 10,000 cells were analyzed by using the flow cytometer (FACSCantoII, BD Biosciences) in FL1 (535 nm) and FL2 channels (>550 nm) for FITC and PI, respectively. Four distinct cell populations were clearly distinguishable from the quadrant gating viz viable (lower left quadrant, AnnexinV-$FITC^-PI^-$), early apoptotic (lower right quadrant, AnnexinV-$FITC^+PI^-$), late apoptotic and early necrotic (upper right quadrant, AnnexinV-$FITC^+PI^+$), and late necrotic (upper left quadrant, AnnexinV-$FITC^-PI^+$). The results were analyzed using FACSDiva software. Tf-R-mediated endocytosis of Tf-C-SLN was confirmed from the receptor blocking experiment where cell surface Tf-R were blocked by treatment of cells with excess amount of free Tf for 1 h prior to the treatment with Tf-C-SLN (4 μM for 24 h).

2.10 Cell cycle analysis

Degradation of DNA is an important parameter of detection of apoptosis (Weir et al. 2007). Cell phase distribution was assayed by the determination of DNA contents. In brief, cells (1×10^6/75 cm^2 flask) were allowed to attach for 24 h and treated with CSSS, C-SLN and Tf-C-SLN (2 and 4 μM curcumin/well) using SS and B-SLN as the respective controls for 24 h at 37 °C in CO_2 incubator. Cells were harvested by centrifugation after treatment, washed with PBS two to three times and fixed in 70 % ethanol for 2 h. The cells were then centrifuged, washed and resuspended in 500 μl PBS containing RNase (100 μg/ml) at room temperature for 30 min. Cellular DNA was then stained with PI (50 μg/ml) and kept in dark for 30 min to stain DNA. The cell cycle was analyzed by a flow cytometer (FACSCantoII) flow cytometer (BD Biosciences) in red (FL2) channel at more than 550 nm, from 10,000 cells. The percent of subG1 fraction was determined by using FACSDiva software.

2.11 Detection of caspase 3

Caspase activation is an important marker of detection of apoptosis. Initiator caspases (caspases 2, 8, 9, and 10) produce activated effector caspases from cleavage of inactive pro-forms of effector caspases (caspases 3, 6, and 7) which in turn cleave cellular protein substrates to start apoptosis (Skommer et al. 2006; Vermes et al. 2000). Herein, we have detected the induction of caspase 3 using CaspGLOW Red Active Caspase 3 Staining Kit. Red-DEVD-FMK is cell permeable, nontoxic probe which binds irreversibly to the activated caspase 3 in apoptotic cells. The red fluorescence label allows for direct detection of activated caspase 3 in apoptotic cells by flow cytometry. Briefly, SH-SY5Y cells (1×10^6/75 cm^2 flask) were allowed to attach for 24 h and treated with CSSS, C-SLN, and Tf-C-SLN (2 and 4 μM curcumin/well) using SS and B-SLN as the respective controls for 24 h at 37 °C in CO_2 incubator. Cells were collected by trypsinization after treatment, washed three times with PBS and resuspended in wash buffer (1×10^6/ml) by centrifugation at 3,000 rpm for 5 min. Three hundred microliters of this cell suspension was stained with 1 μl Red-DEVD-FMK and incubated for 1 h at 37 °C in CO_2 incubator. After incubation, cells were centrifuged at 3,000 rpm for 5 min to remove the supernatant and cells were resuspended in 0.3 ml wash buffer. Cells were analyzed using flow cytometer (FACSCantoII, BD Biosciences) in FL2 channel. Red fluorescence (FL2) was measured at more than 550 nm, for 10,000 cells. Untreated cells were taken as negative control. An additional control was prepared by adding the caspase inhibitor Z-VAD-FMK at 1 μl/ml to inhibit caspase activation and then stained with Red-DEVD-FMK. All experiments were performed in triplicate and results were expressed as mean±SD (n=3).

2.12 Statistical analysis

All the experiments were performed in triplicate and results were expressed as mean±SD (n=3). Statistical analysis was done by performing Student's t test. The differences were considered significant for p values of <0.05.

3 Results

3.1 Statistical analysis

From the factorial design study the effect of independent variables on dependent variables was observed and is shown in Table 1. Multiple regression analysis of the obtained results was performed using Unistat software (Megalon, USA) and the results are shown in Table 2 (Padamwar and Pokharkar 2006). The data of different coefficient values were fitted in the following equation, and the response surface plots were generated using PCP Disso v 2.08 software (IIPC, PCP, Pune, India).

$$Y = \beta_0 + \beta_1 \times 1 + \beta_2 \times 2 + \beta_{11} \times 1 \times 1 + \beta_{22} \times 2 \times 2 + \beta_{12} \times 1 \times 2 \ldots\ldots \quad (1)$$

Table 1 Factorial design results

Batch	Particle size (mean±SD, nm)	Zeta potential (mean±SD, mV)	Percent drug entrapment (mean±SD, %)
SLN 1	145±0.57[a] 156±0.64[b]	20.7±0.22[a] 15.8±0.13[b]	62.88±0.99
SLN 2	168±0.43[a] 179±0.27[b]	20.2±0.17[a] 15.4±0.14[b]	64.21±0.83
SLN 3	218±0.39[a] 226±0.44[b]	19.7±0.13[a] 14.9±0.11[b]	67.11±0.42
SLN 4	158±0.55[a] 165±0.56[b]	17.5±0.22[a] 13.5±0.19[b]	82.32±0.89
SLN 5[c]	188±0.97[a] 194±0.89[b]	16.8±0.33[a] 12.43±0.26[b]	84.99±0.73
SLN 6	221±0.6[a] 229±0.41[b]	16.4±0.11[a] 12.1±0.17[b]	85.91±0.64
SLN 7	164±0.41[a] 172±0.66[b]	14.3±0.12[a] 9.6±0.11[b]	86.58±0.78
SLN 8	206±0.99[a] 214±0.75[b]	13.8±0.099[a] 9.3±0.1[b]	87.22±0.85
SLN 9	228±0.54[a] 239±0.48[b]	13.6±0.092[a] 8.9±0.098[b]	89.02±0.66

[a] B-SLN
[b] C-SLN
[c] Optimized batch

3.2 Effect on zeta potential

The effect of two independent variables on zeta potential of both B-SLN and C-SLN was found to be insignificant (data not shown) (Padamwar and Pokharkar 2006). However, the zeta potential values obtained for all the nine batches were in the range of 13.0 to 21.0 and 8.0 to 16.0 mV for B-SLN and C-SLN respectively indicating the formation of SLN with good stability (Table 1). The ζ potential of C-SLN was 12.43±1.58 mV (Fig. 1a) which shifted towards more negative side after the conjugation of Tf because of the neutralization of amine group of DSPE with Tf. The ζ potential of Tf-C-SLN was 8.21±0.89 mV (Fig. 1b).

3.3 Effect on particle size and PDE

The particle size obtained for all the nine batches of B-SLN were in the range of 140–230 nm while that of C-SLN was 150–240 nm indicating the slight increase in particle size

Table 2 Results of multiple regression analysis for measured responses

Parameters	Coefficients							
	β_0	β_1	β_2	β_{11}	β_{22}	β_{12}	r^2	p
Particle size (B-SLN)	188.44	11.16	33.33		–	–	0.971	0.03
Particle size (C-SLN)	197.11	10.66	33.50		–	–	0.9782	0.02
PDE	84.406	11.33	1.71	−8.136	–	–	0.9982	0.02

with the addition of curcumin (Table 1). The PdI values for all the batches of B-SLN and C-SLN were less than 0.2 indicating the homogeneity of SLN. Hence, the surface response plots were generated by putting the different coefficient values (Table 2) for particle size of B-SLN and C-SLN in Eq. (1) to understand the effect more precisely (Fig. 2a, b).

The effect of both the independent variables on the particle size of SLN was found to be significant. The increase in particle size with increase in both the independent variables can be attributed to the increasing solid content used for the formation of SLN. Thus, both the independent variables significantly affect the particle size of B-SLN (r^2=0.971) as well as C-SLN (r^2=0.978) (Table 2). The mean particle size of C-SLN was found to be 194±2.89 nm with a PdI of 0.15 (Fig. 3a). There was no significant change in particle size after Tf conjugation. The particle size of Tf-C-SLN was found to be 206±3.2 nm with a PdI of 0.18 (Fig. 3b).

The effect of both the independent variables on PDE in C-SLN was observed from the factorial design (Padamwar and Pokharkar 2006). It was observed that increase in amount of HSPC+Chol lead to increased PDE. But, the effect of stabilizer concentration was found to be less significant compared with weight ratio of lipids as seen from the respective coefficient values of both independent variables (Table 2). From the data of multiple regression analysis

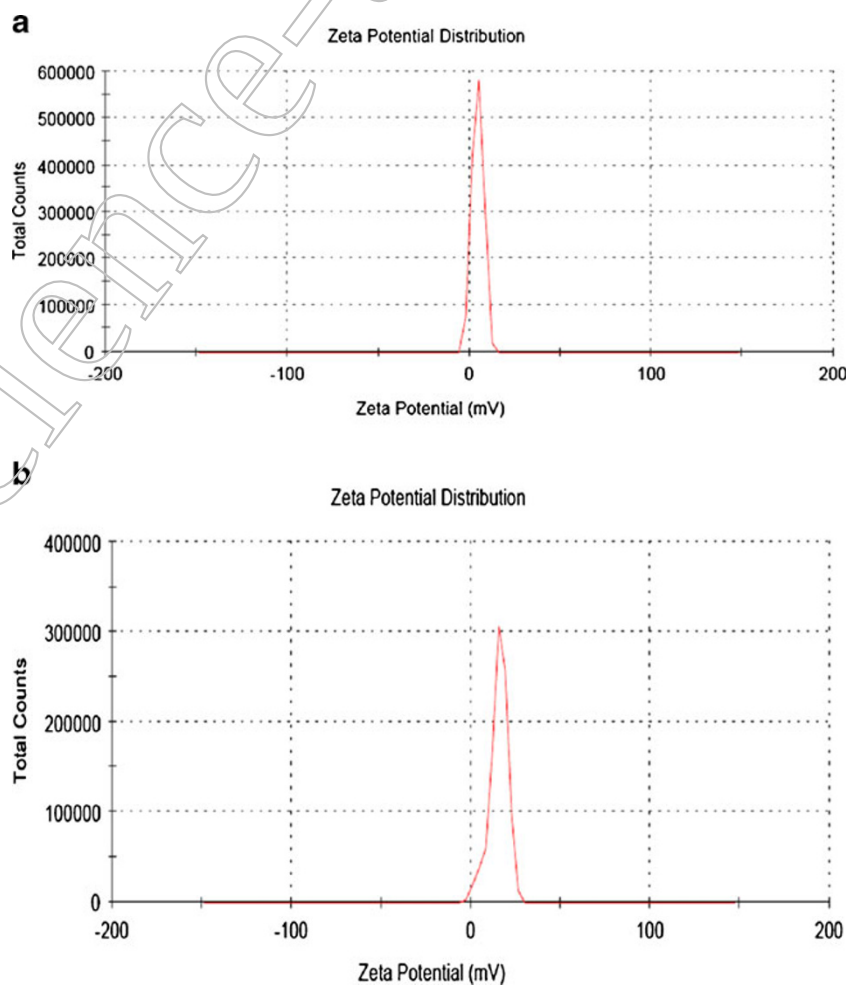

Fig. 1 Zeta potential measurement of C-SLN (**a**) and Tf-C-SLN (**b**)

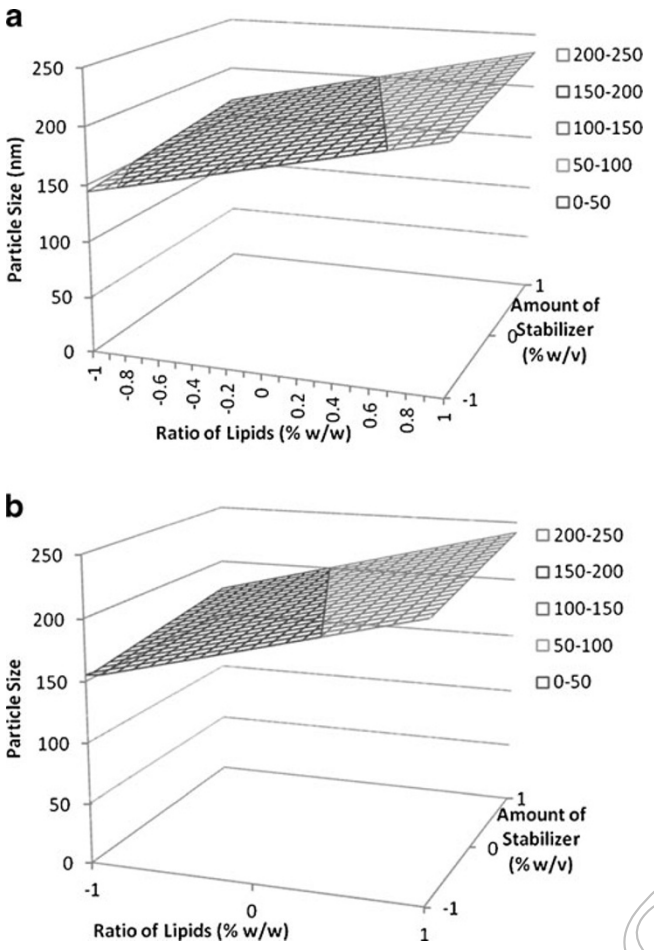

Fig. 2 Surface response plots of effect of independent variables on the particle size of B-SLN (**a**) and C-SLN (**b**)

(Table 2), it was confirmed that both the independent variables have significant effect on the PDE of C-SLN (r^2= 0.99). The surface plot was generated by fitting the different coefficient values (Table 2) for PDE of C-SLN nanoparticles in Eq. (1) (Fig. 4).

The particle size and PDE of B-SLN and C-SLN were found to be increasing with increase in both the variables. Hence, for the determination of optimized batch, PDE was taken as the ultimate deciding dependent variable with optimum particle size. The PDE of C-SLN was determined by ultracentrifugation and it was found to be 77.27±2.34 % indicating good encapsulation efficiency of the prepared SLN.

3.4 Characterization of optimized C-SLN and Tf-C-SLN

The conjugation efficiency was found to be 21.59 mg Tf per mM phospholipids. It was found that the method was highly efficient for the conjugation of Tf by quantifying the actual amount of Tf conjugated on the surface of SLN (Mulik et al. 2010). Morphological characterization using TEM showed spherical nature of nanoparticles (Fig. 1 in the Electronic supplementary material (ESM)).

3.5 Stability study

The stability study showed increased stability of curcumin against photodecomposition in SLN compared with CSSS. The percentage curcumin remained in C-SLN after 3 and 6 months was significantly more compared with that in CSSS (Fig. 2 in the ESM). There was no significant difference in the particle size and zeta potential of C-SLN after 6 months indicating the good physical stability of the prepared SLN (Table 3). These results of particle size, ζ potential, PDE, and curcumin stability showed good efficiency of the method used for the formulation of SLN and their stable nature.

3.6 1H NMR study

1H NMR spectra of CSSS (Fig. 7) showed typical peaks corresponding to curcumin structure. Doublet (2H) at 7.51 ppm for CH=C (1,7-H, alkene, trans) and multiplet at 7.10 ppm for 6-ArH (2H) was observed. 2,5-ArH (4H) were found as multiplet at 6.88 ppm. Doublet (2H) at 6.49 ppm showed presence of =CH–CO (2,6-H, alkene, trans). 1H proton of hydroxyl group of enolate occurred at 5.8 ppm. Singlet at 3.88 ppm indicate 6H and 3H of 3- and 4-ArOCH3 (Bong 2000).

No peaks of curcumin were observed in the spectra of C-SLN indicating the encapsulation of curcumin inside the nanoparticles either in the form of molecular dispersion or amorphous form (Fig. 5). No significant difference was observed in the NMR spectra of both B-SLN and C-SLN indicating that curcumin is not affecting the structure and formation of SLN.

3.7 Differential scanning colorimetry

Differential scanning colorimetry (DSC) of CSSS, B-SLN, and C-SLN was carried out to confirm the complete polymerization of monomer and entrapment of curcumin inside the nanoparticles in molecular dispersion form. The DSC graphs of all the samples are shown in Fig. 6. The T_g of CSSS was found to be 178 °C while that of B-SLN and C-SLN was 79 and 80 °C, respectively. From the graph of curcumin-loaded nanoparticles, it was clear that curcumin was entrapped inside the nanoparticles and that too in molecular dispersion form as no peak for curcumin was obtained. The ΔH values for CSSS, B-SLN and C-SLN were 823.23, 353.97, and 344.18 J/g, respectively. From these ΔH values, it was clear that prepared B-SLN and C-SLN nanoparticles needed less energy for melting compared with CSSS suggesting that curcumin must be entrapped

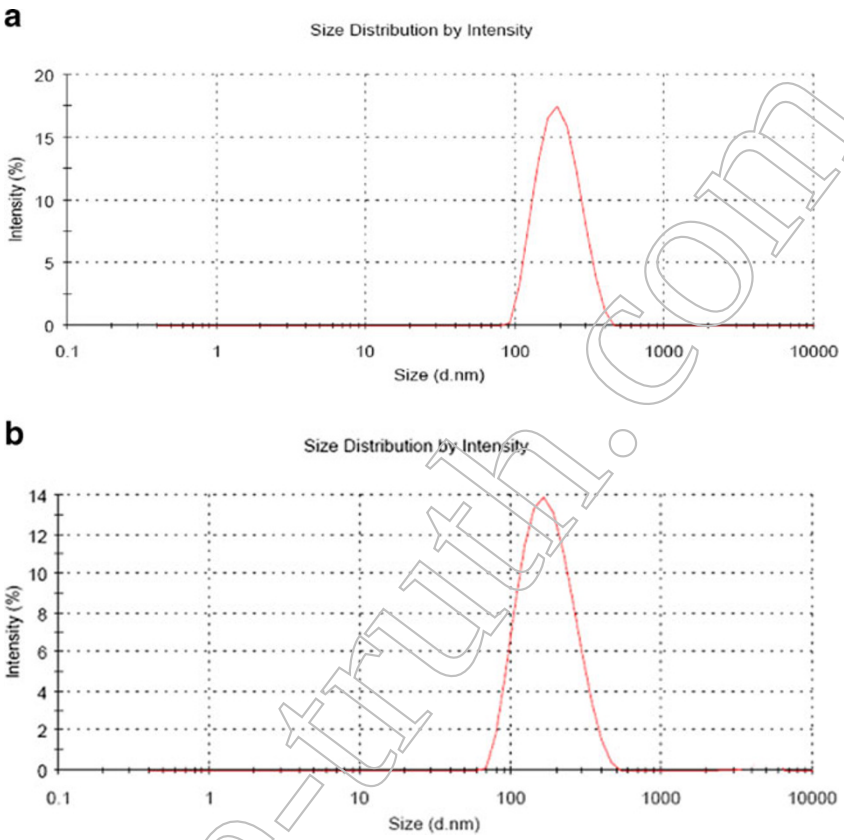

Fig. 3 Particle size measurement of C-SLN (**a**) and Tf-C-SLN (**b**)

inside the SLN and that too in molecular dispersion form (Reddy and Murthy 2004).

3.8 Antiproliferative activity

Antiproliferative activity of curcumin was found to be increasing with dose (Fig. 7a). At concentrations above 8 μM, significant difference in cell viability was observed between CSSS and C-SLN. However, with Tf-C-SLN, even the lowest dose (2 μM) was found to be effective in reducing cell viability significantly compared with CSSS and C-SLN.

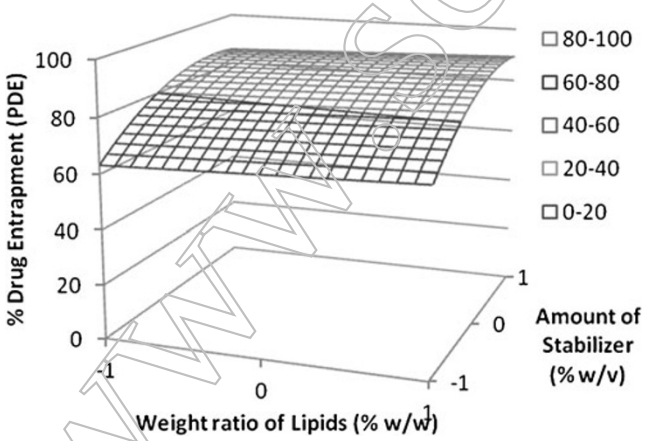

Fig. 4 Surface response plot of effect of independent variables on percent drug entrapment of C-SLN

Cell viability at 2 μM was 98.7±2.1 and 85.07±2.3 % for CSSS and C-SLN respectively while for Tf-C-SLN it was reduced to 36.46±2.4 % showing significantly enhanced anticancer effect. At 4 μM dose, the effect was even more pronounced with Tf-C-SLN (18.8±1.2 %) compared with CSSS (93.9±2.4 %) and C-SLN (80.44±1.3 %), respectively, showing higher potency of Tf-C-SLN. With the highest dose (64 μM), CSSS and C-SLN showed reduction in cell viability upto 28.91±1.5 and 12.45±1.7 % respectively which was achieved wiith 4 μM dose of Tf-C-SLN indicating the significantly enhanced antiproliferative effect. Moreover, we investigated the effect of Tf-C-SLN on HCN-2 (normal neuronal cell line). We observed negligible toxicity (<4 %) on HCN-2 cells at the highest concentration of curcumin (64 μM) used in our study (data not shown). Hence, normal neuronal cells data are not shown in further experiments too.

From receptor-blocking experiment, it was observed that addition of excess free Tf with Tf-C-SLN significantly reduced the antiproliferative activity of Tf-C-SLN. The cell viability after 24-h treatment with Tf-C-SLN was 18.8± 1.2 %, compared with 55.6±1.3 % with Tf-C-SLN+free Tf.

The effect of treatment time on the antiproliferative activity of SLN was also studied using 4 μM curcumin concentrations (Fig. 7b). It was observed that there was not much difference in cell viability after 3- and 6-h treatment with all formulations. However, at later time points, Tf-C-SLN reduced the

Table 3 Stability study of curcumin-loaded SLN

Condition	Particle size (mean±SD, nm)	Polydispersity Index (mean±SD)	Zeta potential (mean±SD, mV)
40 °C/75 % RH in absence of sunlight			
3 months	182±0.89[a]	0.138±0.012[a]	16.18±0.076[a]
	197±0.77[b]	0.147±0.014[b]	14.38±0.067[b]
6 months	194±0.82[a]	0.142±0.012[a]	15.91±0.077[a]
	216±0.97[b]	0.151±0.014[b]	14.11±0.055[b]
40 °C/75 % RH in presence of sunlight			
3 months	180±0.91[a]	0.141±0.013[a]	15.82±0.065[a]
	194±0.79[b]	0.151±0.014[b]	14.24±0.045[b]
6 months	196±0.83[a]	0.147±0.018[a]	15.77±0.043[a]
	211±0.89[b]	0.154±0.011[b]	14.08±0.054[b]

[a] B-SLN
[b] C-SLN

cell viability considerably more than C-SLN. C-SLN was significantly more effective (after 24 and 48 h) than CSSS indicating the sustained release effect of SLN (Fig. 7b). In both dose- and time-dependent studies, SS and B-SLN were taken as respective controls for CSSS and C-SLN. These controls showed negligible effect on cell viability (Fig. 7a, b) showing the antiproliferative effect observed with all the three formulations were indeed because of curcumin.

3.9 Cell uptake study

The drug levels in CSSS-, C-SLN-, and Tf-C-SLN-treated cells after 12 h were 0.85±0.21, 1.4±0.14, and 2.35±0.11 μg/10^5 cells, respectively. Drug levels were found to be decreasing with time in case of CSSS as opposed to C-SLN and Tf-C-SLN wherein the drug levels were found to be increasing. The drug levels after 24 h were 0.65±0.11, 1.52±0.2, and 2.4±0.1 μg/10^5 cells in CSSS, C-SLN, and Tf-C-SLN, respectively. Reduction in drug levels of CSSS-treated cells was more significant (0.53±0.06 μg/10^5 cells) compared with C-SLN-treated cells (1.59±0.1 μg/10^5 cells) and Tf-C-SLN-treated cells (2.42±0.12 μg/10^5 cells) after 48-h treatment. Drug levels from Tf-C-SLN were found to be significantly lower in blocked cells (0.8±0.1/10^5 cells) compared with unblocked cells (2.28±0.13/10^5 cells) in receptor blocking experiment. Tf-C-SLN-treated cells showed higher drug uptake at all time points compared with CSSS- and C-SLN-treated cells.

Fluorescence microscopy of CSSS, C-SLN, and Tf-C-SLN revealed enhanced and sustained uptake from C-SLN and Tf-C-SLN compared with CSSS (Fig. 8b). Fluorescence intensity was found to be reducing with time in case of CSSS suggesting the possible efflux of curcumin with time and noncapability of sustained release (Ganta and Amiji 2009). With C-SLN and Tf-C-SLN, the fluorescence intensity increased after 6 h and it remained almost steady even

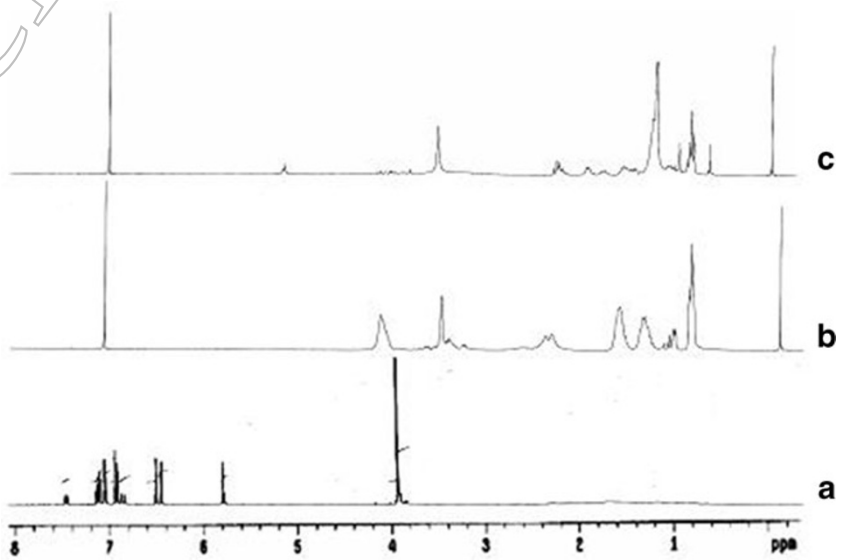

Fig. 5 NMR study. **a** CSSS, **b** C-SLN, and **c** B-SLN

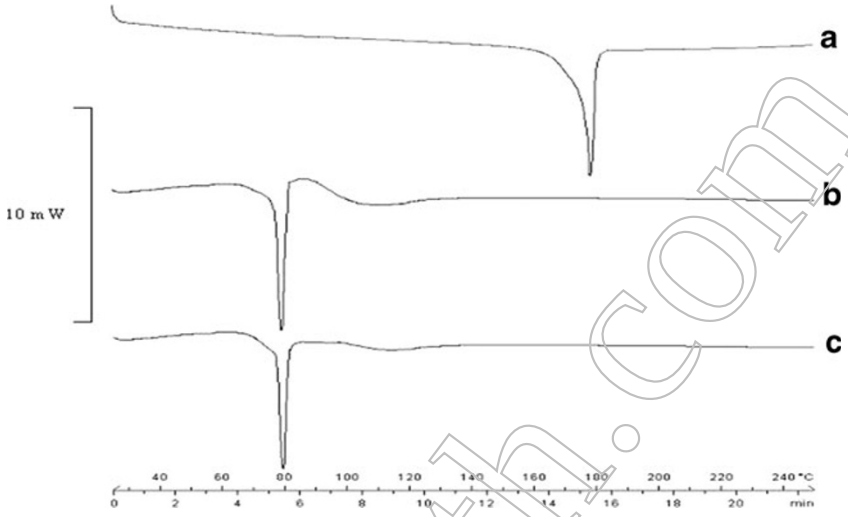

Fig. 6 DSC. **a** CSSS, **b** C-SLN, and **c** B-SLN

after 48 h, suggesting the sustained intracellular release and retention of encapsulated curcumin from SLN localized inside the cells. Fluorescence intensity of Tf-C-SLN-treated cells was more after 24 and 48 h compared with C-SLN-treated cells suggesting receptor-mediated endocytosis. On the contrary, SLN showed enhanced fluorescence intensity compared with CSSS even after 48-h treatment. Images of untreated cells were also taken to see possible autofluorescence. No autofluorescence was observed in untreated control cells.

3.10 Measurement of ROS generation

We also investigated the effect of all formulations on generation of ROS in dose- and time-dependent manner. C-SLN and Tf-C-SLN induced higher ROS compared with CSSS with every dose (Fig. 9a). However, Tf-C-SLN clearly showed significantly increased ROS generation compared with CSSS and C-SLN. SS and B-SLN showed negligible effect on ROS generation (Fig. 9a, b) confirming the effect was indeed because of curcumin.

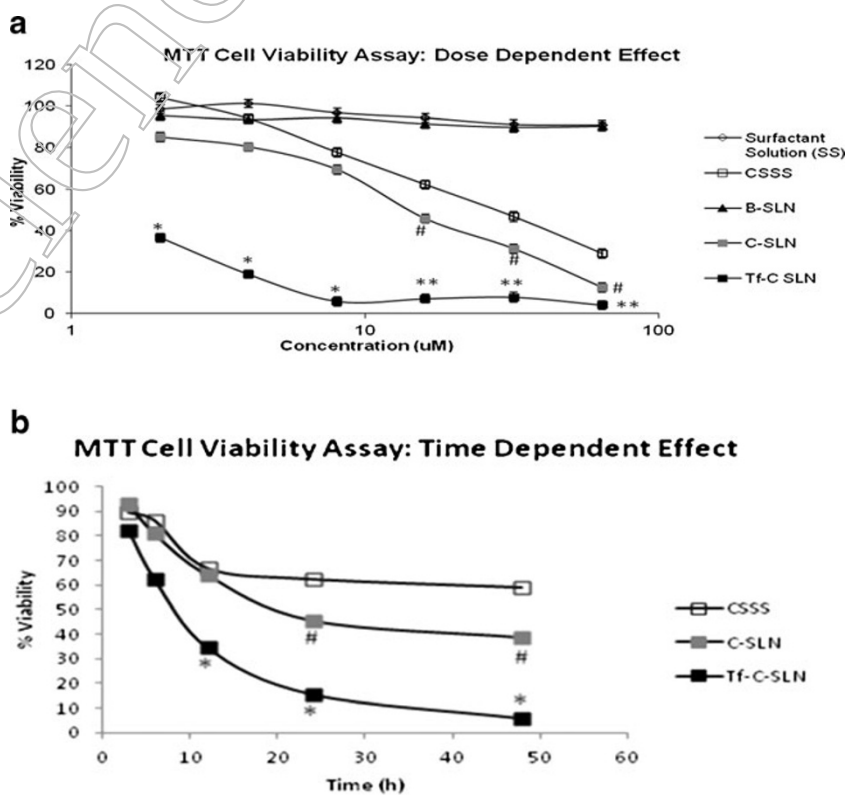

Fig. 7 MTT cell viability assay. **a** Dose-dependent cytotoxicity—SH-SY5Y cells were treated with different concentrations of CSSS, C-SLNs, Tf-C-SLNs, SS, and B-SLNs. The extent of growth inhibition was measured after 24 h by performing MTT assay. *Data* are represented as mean±SD (n=3). *p<0.005, Tf-C-SLN vs. C-SLN and CSSS; **p<0.05, Tf-C-SLN vs. C-SLN and CSSS; #p<0.05, C-SLN vs. CSSS. **b** Time-dependent cytotoxicity—SH-SY5Y cells were treated with 4 μM dose of CSSS, C-SLN, and Tf-C-SLN. The extent of growth inhibition was measured after predetermined time points of 3, 6, 12, 24, and 48 h by performing MTT assay. *Data* are represented as mean±SD (n=3). *p<0.05, Tf-C-SLNs vs. CSSS and C-SLN; #p<0.05, C-SLN vs. CSSS

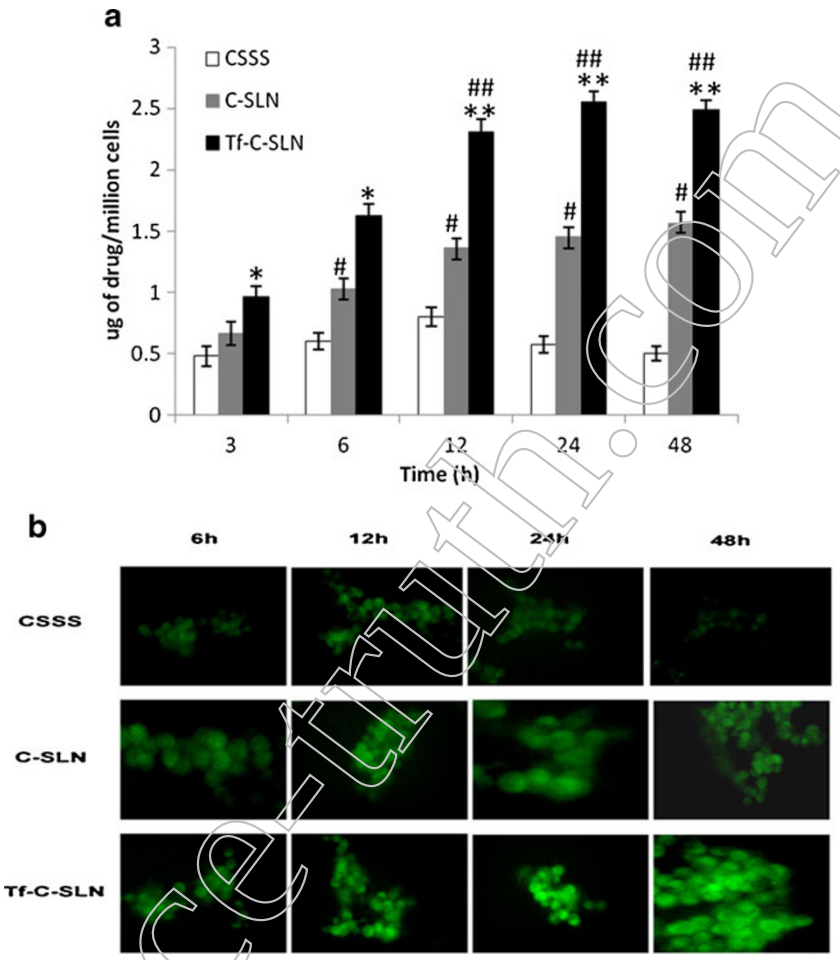

Fig. 8 Cell uptake study. **a** Quantitative intracellular uptake of curcumin from CSSS, C-SLN, and Tf-C-SLN by SH-SY5Y cells. Cells were treated with 10 μM dose. Data as mean ±SD (n=3). *p<0.05, Tf-C-SLN vs. CSSS; **p<0.005, Tf-C-SLN vs. CSSS; #p<0.05, C-SLN vs. CSSS; ##p<0.05, Tf-C-SLN vs. C-SLN. **b** Qualitative cell uptake measurement by fluorescence microscopy

Furthermore, it was observed that excessive addition of free Tf with Tf-C-SLN significantly reduced ROS generation with Tf-C-SLN indicating the effect of Tf receptor blocking and hence, reduced uptake of Tf-C-SLN. Hence, the uptake mechanism of Tf-C-SLN by Tf-R-mediated endocytosis was confirmed. Tf-C-SLN was found to enhance ROS generation significantly compared with CSSS and C-SLN with time (Fig. 9b). C-SLN showed significantly higher ROS generation compared with CSSS after 12-h treatment.

3.11 Cell death analysis

PS externalization as a result of loss of plasma membrane asymmetry is an indicator of apoptosis. Autofluorescence of curcumin was checked using treated unstained cells. The signal observed at 2 and 4 μM was very weak confirming the non-interference of curcumin (Skommer et al. 2006). Tf-C-SLN-treated cells showed 66.4, 24.5, and 45.8, and 49.7 % of early apoptotic (AnnexinV-FITC$^+$PI$^-$) and late apoptotic/early necrotic (AnnexinV-FITC$^+$PI$^+$) populations respectively, compared with CSSS (15.4 and 10.2 and 18.7 and 15.8, respectively) and C-SLN-treated (24.7 and 14.6 and 32.6 and 29.6 %, respectively) cells at 2 and 4 μM dose for 24 h (Fig. 10a, b) indicating enhanced anticancer effect.

At 4 μM concentration, an increase in late apoptotic population was observed with all formulations. The percentage of early apoptotic (AnnexinV-FITC$^+$PI$^-$) and late apoptotic/early necrotic (AnnexinV-FITC$^+$PI$^+$) populations in cells treated with CSSS, C-SLN, and Tf-C-SLN at 2 and 4 μM dose after 48 h treatment were 21.4 and 9.7 and 22.3 and 19.8; 30.2 and 15.6 and 36.1 and 32.4 %; 48.7 and 42.3 and 72.4 and 25.6 %, respectively (Fig. 10b) showing enhanced effect of Tf-C-SLN.

Both SS and B-SLN showed negligible apoptotic effect indicating the apoptosis induced by all the formulations was indeed because of curcumin. It was clearly evident from the results of Tf-R blocking experiment that blocking significantly reduced apoptotic effect of Tf-C-SLN (9.1 % and 7.3 % of early apoptotic (AnnexinV-FITC$^+$PI$^-$) and late apoptotic/early necrotic (AnnexinV-FITC$^+$PI$^+$) populations respectively), confirming the role of Tf-R-mediated endocytosis in enhanced apoptotic activity of Tf-C-SLN.

In C-SLN- and Tf-C-SLN-treated cells early apoptotic (AnnexinV-FITC$^+$PI$^-$) cells were significantly more

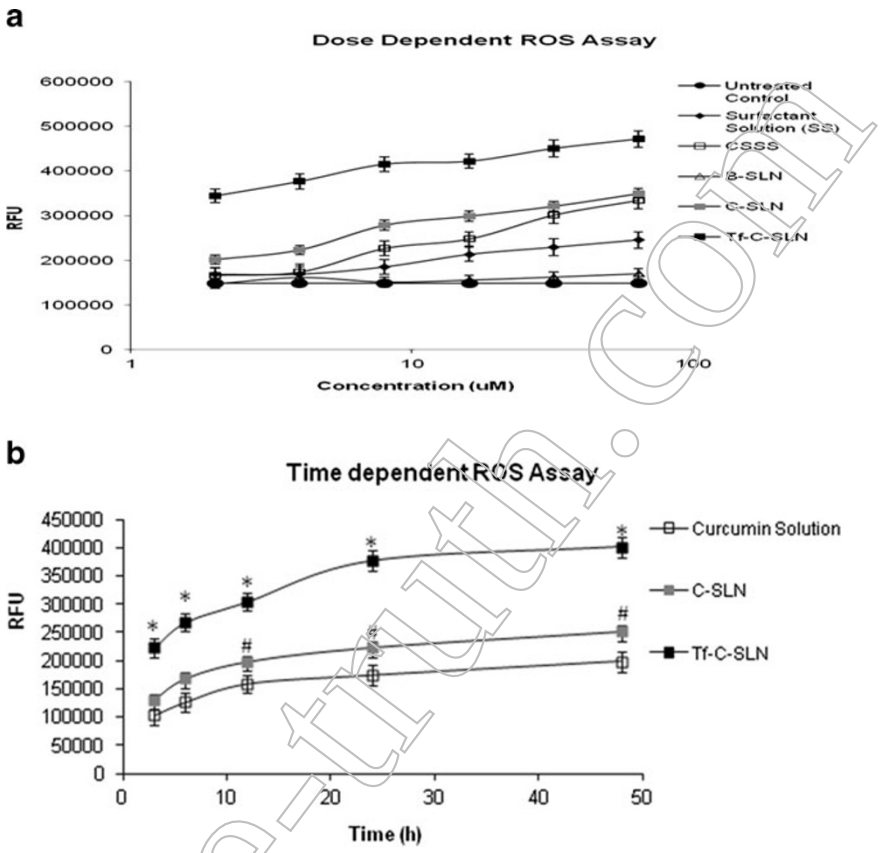

Fig. 9 Measurement of ROS. **a** Effect of dose on generation of ROS by CSSS, C-SLNs, Tf-C-SLNs, SS, and B-SLN in SH-SY5Y cells after 24-h treatment was determined by ROS assay using H2DCF-DA. Data as mean±SD (n=3). *p<0.05, Tf-C-SLNs vs. C-SLN and CSSS; #p<0.05, C-SLN vs. CSSS. **b** Effect of time of treatment on generation of ROS by CSSS, C-SLN, and Tf-C-SLN. SH-SY5Y cells were treated with all formulations (4 μM curcumin) and generation of ROS was determined at predetermined time points of 3, 6, 12, 24, and 48 h. Data as mean±SD (n=3). *p< 0.05, Tf-C-SLNs vs. C-SLN and CSSS; #p<0.05, C-SLN vs. CSSS

compared with late apoptotic/early necrotic cells (AnnexinV-FITC$^+$PI$^+$) at 2 μM dose after 24 h treatment. However, with increase in dose (4 μM) and time (48 h), populations of early apoptotic (AnnexinV-FITC$^+$PI$^-$) and late apoptotic/early necrotic (AnnexinV-FITC$^+$PI$^+$) cells become almost identical suggesting the progression from early apoptotic to late apoptotic/early necrotic population.

3.12 Cell cycle analysis

Cell cycle damage is one of the prime features of apoptotic cells. Presence of hypodiploid peak in the subG1 region is confirmation of apoptosis (Weir et al. 2007). The effect of dose by tracking the percentage of subG1 fraction was determined by FACSDiva software. Tf-C-SLN-treated cells showed significantly more percentage of DNA content in subG1 phase compared with CSSS- and C-SLN-treated cells. At 2 μM dose, the subG1 fraction in CSSS-, C-SLN-, and Tf-C-SLN-treated cells were 14.6, 24.5, and 49.8 %, respectively, which increased to 18.7, 37.5, and 66.5 %, respectively at 4 μM dose (Fig. 11). Hence, it was confirmed that Tf-C-SLN was more efficient in apoptosis induction compared with CSSS and C-SLN. SS and B-SLN showed negligible effect indicating the non-toxic nature of vehicle controls.

3.13 Detection of caspase 3

Caspase 3 is one of the major effector caspase in caspase cascade which ultimately induces apoptosis. Curcumin is known to induce apoptosis in neuroblastoma cells via caspase pathway. At 2 μM curcumin concentration, percentages of caspase 3-positive cells in CSSS-, C-SLN-, and Tf-C-SLN-treated cells were 19.7, 32.4, and 51.2 %, respectively which increased to 26.7, 47.6, and 69.7 %, respectively, at 4 μM dose (Fig. 12). Tf-C-SLN-treated cells showed more percentage of caspase 3-positive cells compared with CSSS- and C-SLN-treated cells with both doses. Both SS and B-SLN showed negligible effect on expression of caspase 3 indicating their nontoxic nature.

4 Discussion

Promising therapeutic efficacy of curcumin against cancer (Anand et al. 2008; Chattopadhyay et al. 2004) always gets hampered due to certain shortcomings such as, low oral bioavailability (Anand et al. 2007) and photodecomposition (Ansari et al. 2005). Systemic administration of curcumin for cancer therapy is also not advisable owing to its uptake by mononuclear phagocytic system being lipophilic in

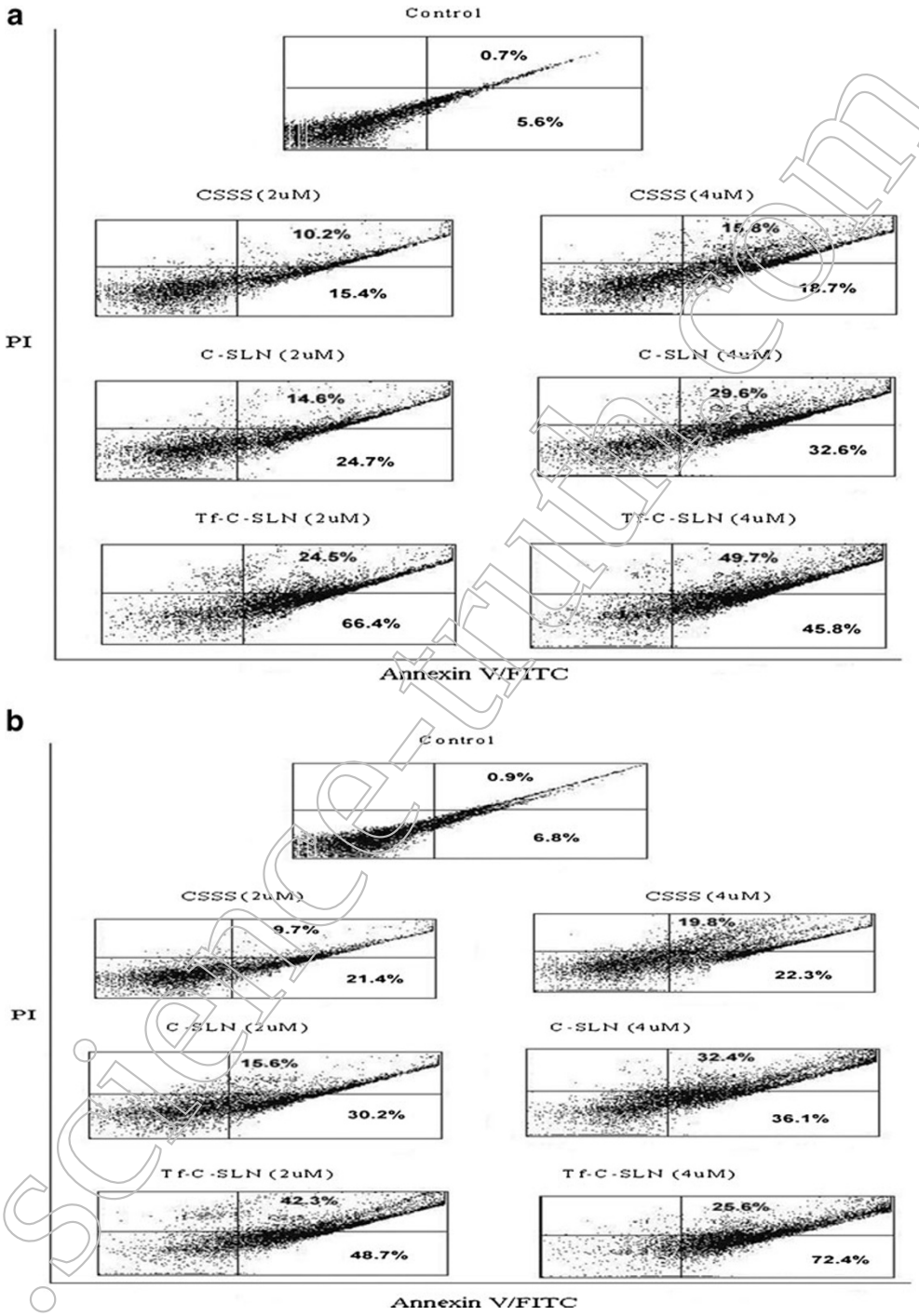

Fig. 10 Measurement of apoptosis in SH-SY5Y cells after 24- (**a**) and 48-h (**b**) treatment with different formulations of curcumin using 2 and 4 μM concentrations

nature and actual drug reaching the target tumor sites such as neuroblastoma will be very less. Hence, there is a compelling need to develop site-specific targeted delivery system of curcumin capable of overcoming the aforementioned shortcomings. Numerous investigations have been done in the past to elucidate therapeutic potential of curcumin and/or curcuminoids against cancer using in vitro cell culture techniques. However, all these investigations are based on solution form of curcumin using organic solvents (DMSO, ethanol, and methanol) and aqueous solutions. Being highly photosensitive, use of solution form of curcumin is not advisable and in vivo use of organic solvents is not recommended for any therapy. The use of transferrin-mediated targeted nanoparticulate drug delivery for the treatment of neuroblastoma is not reported till date which can effectively bypass the aforementioned drawbacks. Physicochemical properties of any formulation play significant role in its overall performance in vitro and in vivo. Dynamic light scattering properties affects physical stability, biodistribution, release pattern, and cellular uptake of nanoparticles.

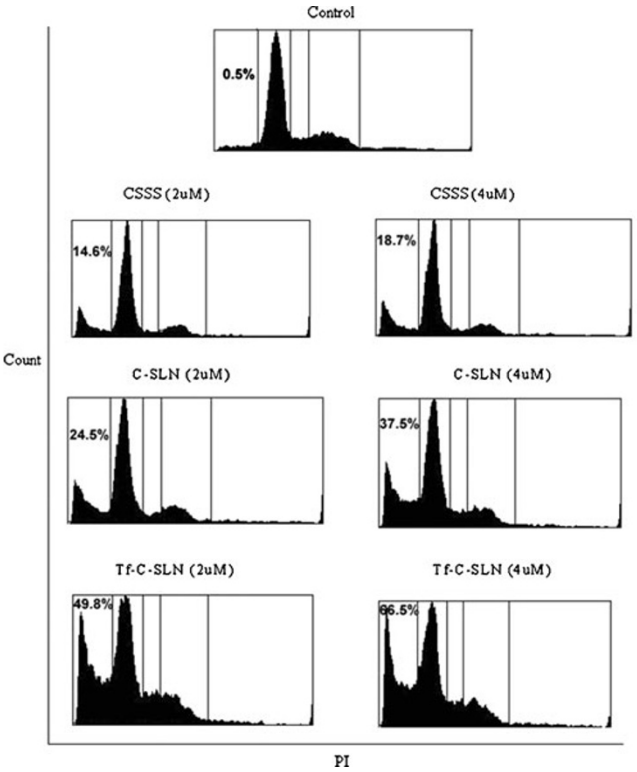

Fig. 11 Cell cycle analysis. Cells were treated with different concentrations of curcumin

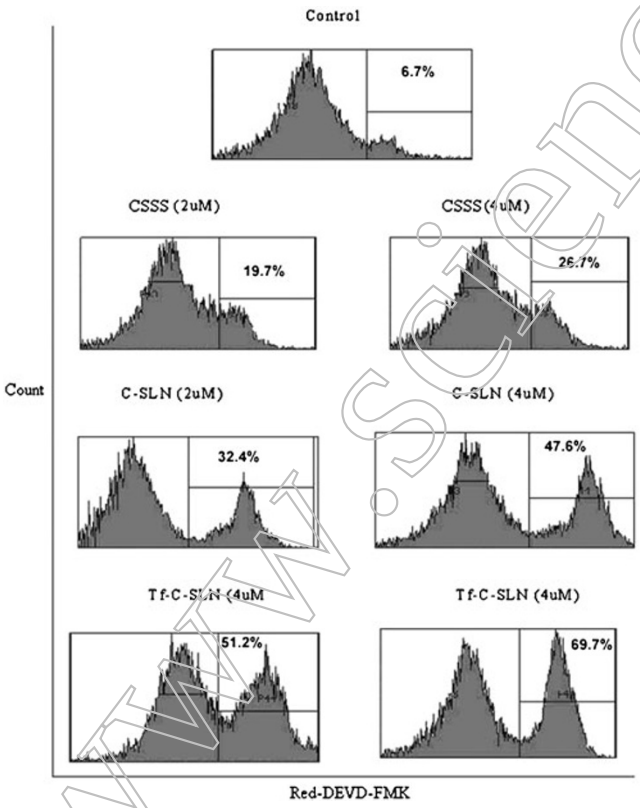

Fig. 12 Detection of caspase 3 expression. Cells treated with different formulations of SLNs

The encapsulation of curcumin inside the SLN in an amorphous or molecularly dispersed form was confirmed by NMR and DSC analysis.

It was observed that Tf-C-SLN has significantly more antiproliferative activity at lower dose of 2 and 4 μM compared with CSSS and C-SLN. In time course study, both C-SLN and Tf-C-SLN showed prominent effect of time of treatment on their antiproliferative activity compared with CSSS. Tf-C-SLN showed more noticeable difference in antiproliferative activity after 6 h compared with CSSS and C-SLN. The increased antiproliferative activity of Tf-C-SLN was in complete agreement with the hypothesis proposed by Sahoo and Labhasetwar (2005). According to their hypothesis, Tf-conjugated delivery systems could have different intracellular sorting pathway after uptake by Tf receptor-mediated endocytosis compared with unconjugated delivery systems via nonspecific pathway and this could increase the intracellular retention and hence, therapeutic efficacy of the encapsulated drug molecule. Tf receptor blocking was found to be reducing the anticancer activity of Tf-C-SLN in all the assays. The antiproliferative activity of Tf-C-SLN was reduced by 3-fold in Tf receptor-blocked cells compared with unblocked cells confirming the receptor-mediated uptake of Tf-C-SLN by SH-SY5Y cells (Sahoo and Labhasetwar 2005). The effect of treatment time on cellular uptake of curcumin from all formulations was also analyzed qualitatively by fluorescence microscopy. Fluorescence intensity of intracellular curcumin elucidated the increased uptake with Tf-C-SLN compared with CSSS and C-SLN. The reduction in fluorescence intensity with time in CSSS-treated cells suggests the possible efflux of curcumin with time and noncapability of sustained release (Ganta and Amiji 2009). However, both C-SLN and Tf-C-SLN showed significant increase in fluorescence intensity compared with CSSS even after 48-h treatment indicating sustained release of curcumin from nanoparticles. Moreover, increase in fluorescence intensity of Tf-C-SLN-treated cells in comparison with C-SLN-treated cells confirmed the proposed hypothesis of increased drug uptake and retention by Sahoo and Labhasetwar (2005).

Significant reduction in drug levels were observed after 12 h in CSSS-treated cells compared with C-SLN (1.5-fold increase) and Tf-C-SLN-treated (2.5-fold increase) cells in quantitative evaluation. The increase in drug levels of Tf-C-SLN and C-SLN treated cells after 24 h treatment was about 4- and 2-fold, respectively, compared with CSSS-treated cells which further increased to >4- and >3-fold, respectively, after 48 h treatment. Furthermore, Tf-C-SLN-treated cells showed about 2-fold increase in drug levels at all time points compared with C-SLN-treated cells. In case of receptor blocked cells, the uptake of curcumin from Tf-C-SLN was significantly lowered. Curcumin is known to induce apoptosis by increasing ROS generation in cancer cells.

Tf-C-SLN-treated cells showed >3- and >1.5-fold increase in ROS generation compared with CSSS- and C-SLN-treated cells. ROS generation was found to be increasing with time in C-SLN- and Tf-C-SLN-treated cells while in CSSS-treated cells the ROS generation became almost stagnant after 12 h substantiating the results of cell uptake. Tf-C-SLN showed prominent increase in ROS generation with increase in treatment time. Flow cytometric detection of apoptosis also showed enhanced therapeutic potential of Tf-C-SLN compared with CSSS and C-SLN. Moreover, Tf-C-SLN-treated cells showed ~90 % apoptosis at the end of 48-h treatment with 4 μM dose compared with CSSS and C-SLN (30 and 60 %, respectively). These observations can be attributed to the sustained release of curcumin from intracellular SLN over longer period of time (Sahoo and Labhasetwar 2005). One important observation from both dose and time dependent apoptosis study was detection of distinctly more late apoptotic/early necrotic cells (AnnexinV-FITC^{+}PI^{+}) than early apoptotic cells (AnnexinV-FITC^{+}PI^{-}) in CSSS-treated cells which can be attributed to the diffusion and accumulation of curcumin at high concentration directly at the site of action causing more necrosis. Early apoptotic (AnnexinV-FITC^{+}PI^{-}) cells were almost similar or slightly less compared with late apoptotic/early necrotic cells (AnnexinV-FITC^{+}PI^{+}) in C-SLN- and Tf-C-SLN-treated cells in dose dependent study suggesting the slow progression from early apoptotic to late apoptotic/early necrotic population because of slow and sustained release of curcumin. The presence of hypodiploid peak in subG1 region is prime indication of apoptosis (Weir et al. 2007). Tf-C-SLN-treated cells showed >2.5-fold increase in subG1 fraction compared with CSSS-treated cells while >1.5-fold increase compared with C-SLN-treated cells. Hence, increased cellular uptake and increased intracellular retention with Tf-C-SLN compared with C-SLN and CSSS plays significant role in increased therapeutic efficacy of curcumin with Tf-C-SLN (Sahoo and Labhasetwar 2005). Cellular uptake of Tf-C-SLN by Tf receptor-mediated endocytosis is the main influential factor in enhanced anticancer effect of Tf-C-SLN. Hence, from our study, we conclude that developed Tf-conjugated drug delivery system offers innovative and effective therapeutic modality of curcumin in the treatment of neuroblastoma.

5 Conclusions

From the present investigation, we conclude that proposed targeted delivery system is suitable for the therapeutically effective delivery of curcumin being biocompatible and biodegradable system capable of sustained drug release and tumor targeting. The enhanced therapeutic potential of Tf-C-SLN in the treatment of neuroblastoma cells in vitro was confirmed from the increased efficacy of curcumin against SH-SY5Y neuroblastoma cells with Tf-C-SLN. Based on the results of present investigation, we conclude that the proposed transferrin-mediated drug delivery system is worth exploring for other types of cancers like breast, prostate, etc.

Acknowledgments The authors are very much thankful to the Centre for International Mobility (CIMO), Helsinki, Finland for providing the Sitra Fellowship (grant No. 1.10.2008/TM-08-5817/Sitra Fellowship) Also, the authors would like to thank Mr. Markku Taskinen, senior laboratory technician, University of Kuopio for his technical help in the study.

Disclosure The authors have no other relevant affiliations or financial involvement with any organization or entity with a financial interest in or financial conflict with the subject matter or materials discussed in the manuscript apart from those disclosed. No writing assistance was utilized in the production of this manuscript.

References

Adrian JE, Wolf A, Steinbach A, Rössler J, Süss R (2011) Targeted delivery to neuroblastoma of novel siRNA-anti-GD2-liposomes prepared by dual asymmetric centrifugation and sterol-based post-insertion method. Pharm Res 28(9):2261–2272

Aggarwal BB, Harikumar KB (2009) Potential therapeutic effects of curcumin, the anti-inflammatory agent, against neurodegenerative, cardiovascular, pulmonary, metabolic, autoimmune, and neoplastic diseases. Int J Biochem Cell Biol 41:40–59

Aggarwal BB, Kumar A, Bharti A (2003a) Anticancer potential of curcumin: preclinical and clinical studies. Anticancer Res 23:363–398

Aggarwal B, Swaroop P, Protiva P, Raj SV, Shirin H, Holt PR (2003b) Cox-2 is needed but not sufficient for apoptosis induced by Cox-selective inhibitors in colon cancer cells. Apoptosis 8:649–654

Aggarwal BB, Kumar A, Aggarwal MS, Shishodia S (2005a) Curcumin derived from turmeric (*Curcuma longa*): a spice for all seasons. In: Preuss HG (ed) Phytopharmaceuticals in cancer chemoprevention. CRC, Boca Raton, pp 349–387

Aggarwal BB, Shishodia S, Takada Y (2005b) Curcumin suppresses the paclitaxel-induced nuclear factor-{kappa}B pathway in breast cancer cells and inhibits lung metastasis of human breast cancer in nude mice. Clin Cancer Res 11:7490–7498

Anand P, Kunnumakkara AB, Newman RA, Aggarwal BB (2007) Bioavailability of curcumin: problems and promises. Mol Pharm 4:807–818

Anand P, Sundaram C, Jhurani S, Kunnumakkara AB, Aggarwal BB (2008) Curcumin and cancer: an "old-age" disease with an "age-old" solution. Cancer Lett 267:133–164

Ansari MJ, Ahmad S, Kohli K, Ali J, Khar RK (2005) Stability indicating HPTLC determination of curcumin in bulk drug and pharmaceutical formulations. J Pharm Biomed Anal 39:132–138

Azuine MA, Bhide SV (1992) Chemopreventive effect of turmeric against stomach and skin tumors induced by chemical carcinogens in Swiss mice. Nutr Cancer 17:77–83

Bong PH (2000) Spectral and photophysical behaviors of curcumin and curcuminoids. Bull Korean Chem Soc 21(1):81–86

Bradford MA (1976) Rapid and sensitive method for the quantitation of microgram quantities of protein utilizing the principle of protein-dye binding. Anal Biochem 72:248–254

Buttke TM, Sandstrom PM (1994) Oxidative stress as a mediator of apoptosis. Immunol Today 15:7–10

Chattopadhyay I, Biswas K, Bandyopadhyay U, Banerjee RK (2004) Turmeric and curcumin: biological actions and medicinal applications. Curr Sci 87:44–53

Chearwae W, Anuchapreeda S, Nandigama K, Ambudkar SV, Limtrakul P (2004) Biochemical mechanism of modulation of human P-glycoprotein (ABCB1) by curcumin I, II, and III purified from turmeric powder. Biochem Pharmacol 68:2043–2052

Chearwae W, Wu CP, Chu HY, Lee TR, Ambudkar SV, Limtrakul P (2006) Curcuminoids purified from turmeric powder modulate the function of human multidrug resistance protein 1 (ABCC1). Cancer Chemother Pharmacol 57:376–388

Christine SA, Kumari L, Khar A (2004) Effect of curcumin on normal and tumor cells: role of glutathione and bcl-2. Mol Cancer Ther 3:1101–1108

Dehal PK, Embleton MJ, Kemshead JT, Hawkins RE (2002) Targeted cytokine delivery to neuroblastoma. Biochem Soc Trans 30 (4):518–520

Di Paolo D et al (2011) Neuroblastoma-targeted nanoparticles entrapping siRNA specifically knockdown ALK. Mol Ther 19(6):1131–1140

Dilnawaz F, Singh A, Sahoo SK (2012) Transferrin-conjugated curcumin-loaded superparamagnetic iron oxide nanoparticles induce augmented cellular uptake and apoptosis in K562 cells. Acta Biomater 8:704–719

Dorai T, Cao YC, Dorai B, Buttyan R, Katz AE (2001) Therapeutic potential of curcumin in human prostate cancer. III. Curcumin inhibits proliferation, induces apoptosis, and inhibits angiogenesis of LNCaP prostate cancer cells in vivo. Prostate 47:293–303

Ganta S, Amiji M (2009) Coadministration of paclitaxel and curcumin in nanoemulsion formulations to overcome multidrug resistance in tumor cells. Mol Pharm 6:928–939

Gupta Y, Jain A, Jain SK (2007) Transferrin-conjugated solid lipid nanoparticles for enhanced delivery of quinine dihydrochloride to the brain. J Pharm Pharmacol 59:935–940

Gutman RL, Peacock G, Lu R (2000) Targeted drug delivery for brain cancer treatment. J Control Release 65:31–41

Jacobson MD (1996) Reactive oxygen species and programmed cell death. Trends Biochem Sci 21:83–86

Jenning V, Korting MS, Gohla S (2000) Vitamin A-loaded solid lipid nanoparticles for topical use: drug release properties. J Control Release 66:115–126

Joe B, Vijaykumar M, Lokesh BR (2004) Biological properties of curcumin-cellular and molecular mechanisms of action. Crit Rev Food Sci Nutr 44:97–111

Kunwar A, Barik A, Mishra B, Rathinasamy K, Pandey R, Priyadarsini KI (2008) Quantitative cellular uptake, localization and cytotoxicity of curcumin in normal and tumor cells. Biochem Biophys Acta 1780:673–679

Lemieux P, Page M (1994) Sensitivity of multidrug-resistant MCF-7 cells to a transferrin-doxorubicin conjugate. Anticancer Res 14:397–403

Li JL, Wanga L, Liu XY (2009) In vitro cancer cell imaging and therapy using transferrin-conjugated gold nanoparticles. Cancer Lett 274:319–326

Martell LA, Agrawal A, Ross DA, Muraszko KM (1993) Efficacy of transferrin receptor-targeted immunotoxins in brain tumor cell lines and pediatric brain tumors. Cancer Res 53(6):1348–1353

Maruyama K, Ishida O, Kasaoka S (2004) Intracellular targeting of sodium mercaptoundecahydrododecaborate (BSH) to solid tumors by transferrin-PEG liposomes, for boron neutron-capture therapy (BNCT). J Control Release 98:195–207

Mulik R, Mahadik KR, Paradkar AR (2009) Development of curcuminoids loaded poly(butyl) cyanoacrylate nanoparticles: physicochemical characterization and stability study. Eur J Pharm Sci 37:395–404

Mulik RS, Mönkkönen J, Juvonen RO, Mahadik KR, Paradkar AR (2010) Transferrin mediated solid lipid nanoparticles containing curcumin: enhanced in vitro anticancer activity by induction of apoptosis. Int J Pharm 398:190–203

Padamwar MN, Pokharkar VB (2006) Development of vitamin loaded topical liposomal formulation using factorial design approach: drug deposition and stability. Int J Pharm 320:37–44

Page-Clisson ME, Pinto HA, Ourevitch M, Andremont A, Couvreur P (1998) Development of ciprofloxacin-loaded nanoparticles: physicochemical study of the drug carrier. J Control Release 56:23–32

Qian ZM, Li H, Sun H, Ho K (2002) Targeted drug delivery via the transferrin receptor-mediated endocytosis pathway. Pharmacol Rev 54:561–587

Ramachandran C, Fonseca HB, Jhabvala P, Escalon EA, Melnick SJ (2002) Curcumin inhibits telomerase activity through human telomerase reverse transcriptase in MCF-7 breast cancer cell line. Cancer Lett 184:1–6

Reddy LH, Murthy RSR (2004) Influence of polymerization technique and experimental variables on the particle properties and release kinetics of methotrexate from poly(butylcyanoacrylate) nanoparticles. Acta Pharma 54:103–118

Sahoo SK, Labhasetwar V (2005) Enhanced antiproliferative activity of transferrin-conjugated paclitaxel-loaded nanoparticles is mediated via sustained intracellular drug retention. Mol Pharm 2:373–383

Sharma RA, Gescher AJ, Steward WP (2005) Curcumin: the story so far. Eur J Cancer 41:1955–1968

Singh S, Aggarwal BB (1995) Activation of transcription factor NF-kB is suppressed by curcumin (diferulolylmethane). J Biol Chem 270:24995–25000

Skommer J, Wlodkowic D, Pelkonen J (2006) Cellular foundation of curcumin-induced apoptosis in follicular lymphoma cell lines. Exp Hematol 34:463–474

Thangapazham RL, Sharma A, Maheshwari RK (2006) Multiple molecular targets in cancer chemoprevention by curcumin. AAPS J 8:E443–E449

Tivnan A, Orr WS, Gubala V, Nooney R, Williams DE (2012) Inhibition of Neuroblastoma tumor growth by targeted delivery of MicroRNA-34a using anti-disialoganglioside GD_2 coated nanoparticles. PLoS One 7(5):e38129

Tiyaboonchaia W, Tungpradita W, Plianbangchang P (2007) Formulation and characterization of curcuminoids loaded solid lipid nanoparticles. Int J Pharm 337:299–306

Ulbrich K, Hekmatara T, Herbert E, Kreuter J (2009) Transferrin and transferrin-receptor-antibody-modified nanoparticles enable drug delivery across the blood–brain barrier (BBB). Eur J Pharm Biopharm 71:251–256

Veldhoen S, Laufer SD, Restle T (2008) Recent developments in peptide-based nucleic acid delivery. Int J Mol Sci 9:1276–1320

Vermes I, Haanen C, Reutelingsperger C (2000) Flow cytometry of apoptotic cell death. J Immuno Methods 243:167–190

Wang H, Joseph JA (1999) Quantifying cellular oxidative stress by dichlorofluorescein assay using microplate reader. Free Radic Biol Med 27:612–616

Wang F, Jiang X, Yang DC, Elliott RL, Head JF (2000) Doxorubicin-gallium-transferrin conjugate overcomes multidrug resistance: evidence for drug accumulation in the nucleus of drug resistant MCF-7/ADR cells. Anticancer Res 20:799–808

Weir NM, Selvendiran K, Kutala VK (2007) Curcumin induces G2/M arrest and apoptosis in cisplatin-resistant human ovarian cancer cells by modulating Akt and p38 MAPK. Cancer Biol Ther 6:178–184

Widera A, Norouziyan F, Shen WC (2003) Mechanisms of Tfr-mediated transcytosis and sorting in epithelial cells and applications toward drug delivery. Adv Drug Deliv Rev 55:1439–1466

Yang X, Koh CG, Liu S (2009) Transferrin receptor-targeted lipid nanoparticles for delivery of an antisense oligodeoxyribonucleotide against bcl-2. Mol Pharm 6:221–230